ACS Partner Journal
PRECISION CHEMISTRY
pubs.acs.org/PrecisionChem

Article

Nanotube Derived Ordered Carbons Predicted by Neural Network Potential

Shuqi Xie, Kun Ni,* and Yanwu Zhu*

Cite This: https://doi.org/10.1021/prechem.5c00020

ABSTRACT: Searching for novel carbon allotropes with excellent mechanical and interesting electronic properties is valuable, but such a large structural search remains a challenge if purely based on the traditional density functional theory (DFT) combined with Monte-Carlo (MC) methods. Herein, the neural network potential is utilized to accelerate the sampling of the stochastic surface walking algorithm for a global structural search of ordered carbons from carbon nanotubes (CNTs) under pressure. A variety of unreported ordered carbons are obtained, among which CNTs with diameters smaller than 0.7 nm are more sensitive to pressure than bigger tubes. Most ordered carbons obtained show great thermodynamical and kinetic stability, verified by *ab initio* molecular dynamics simulations and phonon spectra. The ordered carbons demonstrate direct or indirect band gaps in the range of 0 to 4.4 eV, including 13 superhard (H_v > 40 GPa) structures and 1 ductile (Pugh's Ratio G/B < 0.57) structure, in which the modulus of ordered carbons exhibits a linear correlation with the density. Our study provides a pathway to create new carbons from nanotubes and a deeper understanding of the structural evolution of CNTs under pressure.

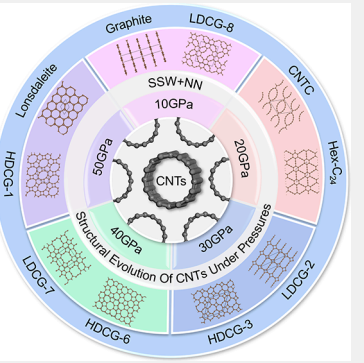

KEYWORDS: *neural network potential, surface walking algorithm, CNTs evolution, novel carbon structures, DFT*

1. INTRODUCTION

With excellent electrical, thermal and mechanical properties, carbon nanomaterials like graphene,[1] fullerenes,[2] and carbon nanotubes (CNTs)[3] are expected to play critical roles in electronic devices, thermal management, energy storage, and so on. Among them, CNTs possess variable diameter and chirality, bringing about abundant physical and chemical properties.[4] On the other hand, studies show that CNTs can agglomerate by covalent bonding, thus constructing new carbons using CNTs as building blocks or precursors has attracted intensive research interest. For example, Merlen et al. compressed single-wall carbon nanotubes (SWNTs) in a diamond anvil and found that SWNTs can be irreversibly transformed into cubic diamonds at a pressure of 14.5 GPa and a temperature of 1800 K.[5] Khabashesku et al. observed the formation of diamond or graphite phases by compressing SWNTs at 8.0 or 9.5 GPa performed in a high pressure chamber.[6] Popov et al. synthesized a superhard phase (SP-SWNT) with hardness comparable to diamond by applying a shear deformation to SWNTs at 24 GPa in a shear diamond anvil cell.[7] Through cold compression of CNTs at ∼ 75 GPa by using a gasket diamond anvil cell, Wang et al. obtained a sp^3-rich hexagonal carbon with an average density of 3.6 ± 0.2 g/cm^3 that can crack diamond.[8]

Despite the experimental process described above, the atomic structures of CNTs-derived carbons remain unclear. To have a deeper understanding into the structural evolution and to predict more carbon structures from CNTs, theoretical studies using CNTs as the precursor have been carried out, mostly based on density functional theory (DFT).[9,10] Hu et al. applied hydrostatic and nonhydrostatic pressure onto zigzag ((4,0), (5,0), (6,0)) and armchair ((2,2), (3,3)) SWNTs through CASTEP[11] and obtained several three-dimensional (3D) SWNT polymers, a.k.a., 3D (4,0) -I, -II, -III and 3D (2,2) -I, -II, -III phases. Among them, 3D (2,2)-II is considered to be like the previously reported bct-C_4 structure.[12] These structures possess many interesting physical properties, such as superhardness, high tensile strength and tunable electronic properties.[13] However, manually applying pressure to the precursor followed by relaxation shows a relatively low sampling efficiency of the potential energy surface (PES), which often restricts the structural search. Combining DFT with structural search algorithms is powerful for novel structure prediction. For instance, based on the particle swarm optimization (PSO) algorithm,[14] which has been extensively used by implementing CALYPSO code,[15] a Cco-C_8 carbon with hardness up to 95.1 GPa has been proposed.[16] The simulated X-ray diffraction pattern, density and bulk modulus of Cco-C_8 agree well with the material experimentally prepared

Received: February 19, 2025
Revised: April 29, 2025
Accepted: April 30, 2025

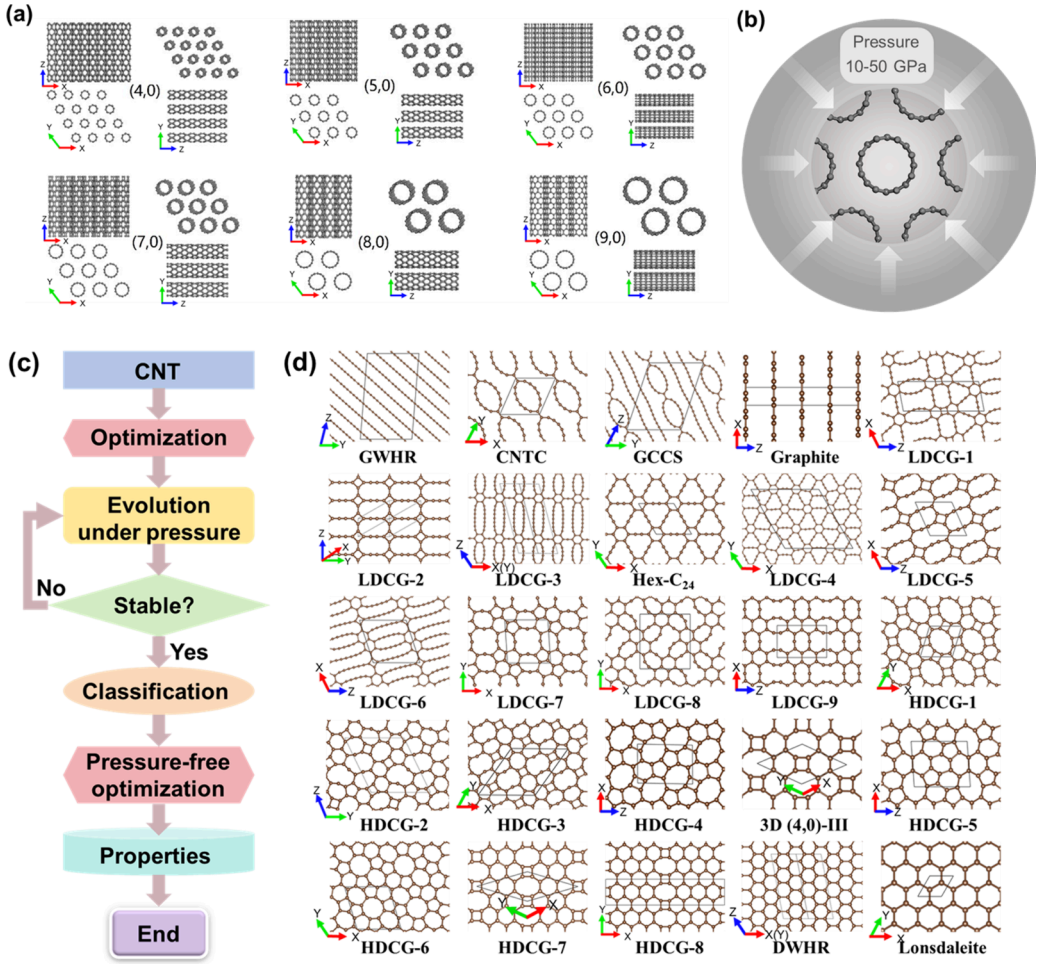

Figure 1. (a) Initial structure of CNT arrays. (b) Schematic diagram of applying the pressure. (c) Research workflow for the structural search of SDCCs. (d) 25 types of SDCCs were obtained from the SSW-NN structural search.

by cold-compressing CNT bundles.[8] With the same method, Zhao et al. used zigzag ($(n,0)$, n = 3−9) and armchair ((n,n), n = 2−4,6) SWNTs as the precursors and obtained eight novel sp^2- and sp^3- hybridized carbon structures: 3D-$(n,0)$ carbon (n = 4,5,7,8,9) and 3D-(n,n) carbon (n = 3,4,6).[17] Hu et al. proposed four superhard carbon structures (L-carbon, CM-carbon, K-carbon, and Cco-C_{160}) derived from (4,4) (7,0) (19,0) (20,0) SWNTs under hydrostatic compression, which are energetically more favorable than Cco-C_8.[18] With high sampling efficiency, the PSO algorithm has been shown to be powerful in structure search but still faces high costs since high-cost DFT-based geometry relaxation is necessary.

Recently, the stochastic surface walking (SSW) method in combination with the neural network potential (NN) developed by Liu et al.[19,20] has shown great potential to improve the sampling efficiency of PES and reduce the calculation costs compared to the PSO+DFT method. Yu et al. identified a novel monoclinic carbon phase (Y carbon) with 4+5+6+7+8 member rings using SSW-NN, showing superhard properties (shear hardness: 81.9 GPa) and stability above 21.5 GPa.[21] Similarly, Zhu et al. employed the SSW method to identify the lowest energy pathway starting from graphite and found a new transition pathway to a disordered phase without forming a nuclei core.[22] With the SSW method combined with a parallel replica exchange algorithm, Zhang et al. have successfully located the global minima (GM) of fullerenes from random atoms without falling into other local minimum structures.[23] With the SSW method, Xie et al. explored the phase transition pathways from graphite to diamond and captured 7 intermediate structures at 15 GPa.[24] Ni et al. obtained plenty of metastable structures derived from C_{60} fullerene crystals using the SSW-NN global searching method.[25] In observation of the low structural searching efficiency from CNTs either experimentally or theoretically, SSW-NN is expected to deal with the large system of CNT bundles for more comprehensive sampling than the traditional DFT+MC methods. In this way, the long-standing issue of the structural evolution from CNTs under high pressures may be addressed.

In this work, we report the first attempt of using the SSW-NN method in investigating the structural evolution of SWNTs under pressures and demonstrate the energy evolution path and corresponding structural sampling. With further DFT calculations, 21 kinetically and thermodynamically stable structures are determined. The obtained SWNTs-derived carbons show abundant electronic properties ranging from metallic to semiconducting and interesting mechanical properties ranging from ductile to superhard. Our work expands the family of SWNTs-derived carbons to tens of thousands of members, providing an avenue to explore the applications of novel carbons with versatile properties synthesized from SWNTs.

https://doi.org/10.1021/prechem.5c00020
Precis. Chem. XXXX, XXX, XXX−XXX

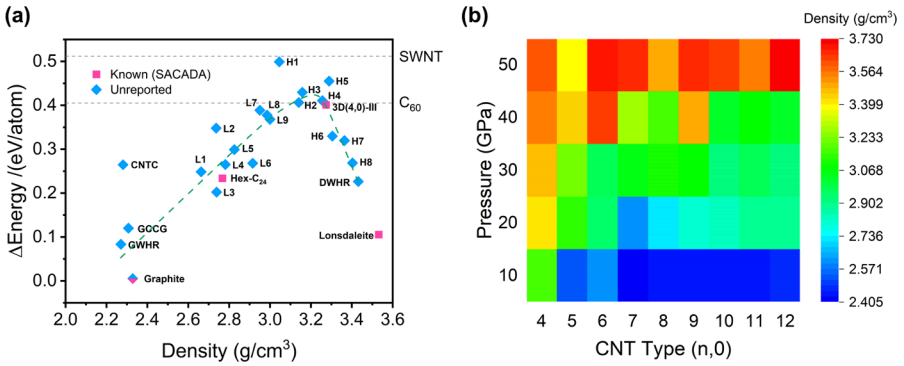

Figure 2. (a) Energy of SDCCs relative to graphite after optimization at 0 Pa (H or L in the figure indicates HDCG or LDCG, respectively). (b) Averaged density of SDCCs obtained at different pressures. The density is calculated by dividing mass of atoms in the unit cell with unit cell volume.

2. METHODS

Six kinds of SWNTs with chiral indices of $(n,0)$ where n = 4−9 were built. The primitive cells were optimized and expanded to a large-scale supercell with about 1,000 atoms, containing a SWNT array with multiple SWNTs as the initial structure for the SSW structural search, as demonstrated in Figure 1a. In order to give more degrees of freedom for the structural evolution, Large-scale Atomic Simulation with neural network Potential software (LASP) was used to perform the SSW algorithm with NN potential.[26,27] All structural search was carried out at 5 pressures: 10, 20, 30, 40, and 50 GPa, as shown in Figure 1b. Each run contained 50−1000 SSW searching steps performed at 300 K. All SSW search was performed in 3 parallel runs, except for those with a chiral index of $(n,0)$ (n = 10−12) with only 1 sampling run to further explore the evolution trend. The end criterion of structural search is the formation of a stable structure with relatively low energy, e.g., diamond, graphite, or other metastable structures, that remain unchanged for another 100 sampling steps. The evolution process was classified according to the final structure; all paths with the same final structure were aggregated together. Finally, 25 types of structures were obtained. The input file for the LASP calculation, e.g., for a hydrostatic pressure of 10 GPa, is shown below.

```
potential NN
explore_type ssw
Ewaldflag 0
%block netinfo
C C.pot
%end block netinfo
PrintChg 0
Run_type 15
SSW.SSWsteps 200
SSW.Temp 300
SSW.pressure 10
SSW.quick_Setting 3
SSW.ftol 1 × 10−2
SSW.ds_atom 2
SSW.output F
SSW.printevery F
SSW.printselect 0
```

The following structural optimization and property calculations were performed using the Vienna Ab initio Simulation Package (VASP).[28] The Perdew−Burke−Ernzerhof (PBE)[29] with generalized gradient approximation (GGA)[30] functional was adopted. Becke−Johnson damping DFT-D3 correction[31] was used. The kinetic energy cutoff for the plane wave basis set was 500 eV. Gamma-centered K-point sampling was used with a spacing of 0.1 $Å^{-1}$ for AIMD simulations, 0.04 $Å^{-1}$ for geometric optimization, and 0.008 $Å^{-1}$ for DOS calculations. The energy convergence value was set as 10^{-8} eV and the force tolerance for geometry optimization was 10^{-4} eV $Å^{-1}$. The spin was unrestricted for all of the calculations. *Ab initio* molecular dynamic (AIMD) simulations at 300 and 1000 K were performed based on the canonical ensemble (NVT) to examine the thermal stability, with a time step of 1 fs for a total time length of 5 ps. Phonon spectra were calculated using the finite displacement method implemented in PHONOPY.[32] The Heyd−Scuseria−Ernzerhof (HSE06) screened hybrid functional[33] was used to calculate electronic band structures. The average Young's modulus, bulk modulus and shear modulus were calculated according to Voigt−Ruess−Hill approximation.[34] The Vickers hardness was estimated using the model developed by Chen et al.[35] High symmetry k-points of Brillouin zone were used in band structure calculations.[36,37] The geometric structures were plotted by VESTA software.[38]

3. RESULT AND DISCUSSION

The simulation gradually loads pressure on an array with multiple SWNTs, as shown in Figure 1a,b. The workflow for the SWNTs structural search is shown in Figure 1c. Six kinds of SWNT arrays were built with indexes of $(n,0)$ where n = 4−9. Based on the SSW-NN method, the evolutionary potential energy surface (PES) of SWNTs was efficiently explored at 10, 20, 30, 40, or 50 GPa. All structural samplings were performed with 3 parallel runs, resulting in 108 LASP sampling runs and 53423 intermediate structures. The energy of the structure relative to the AB stacking graphite at each pressure was calculated and sorted as the initial data set. A total of 25 categories were divided according to the final structure, and about 10 representative structures were selected for each category. More details on structure evolution, including the energy evolution paths and representative intermediate structures for each type of structure, can be found in Figures S1−S25 in Supporting Information. Among the 25 types of final structures, 21 representative structures with different types were selected to further evaluate the electronic and mechanical properties while 4 were not (GWHR, GCCS, LDCG-4, HDCG-2) due to the large size of the system (more than 100 atoms).

Twenty-five different types of obtained SWNTs-derived carbon crystals (SDCCs) are shown in Figure 1d. Those structures with a density less than 3 g/cm^3 are called low-density carbon grids (LDCG); otherwise, they are named as high-density carbon grids (HDCG). The number of atoms in the maximum carbon ring for LDCG is typically greater than 10. The CNT chain is abbreviated as CNTC, the graphite with heterocyclic rings is denoted as GWHR, the diamond with heterocyclic rings is denoted as DWHR, and the composite structure of graphite and carbon nanotube chain is referred to as GCCS. In addition, numbers in the LDCG and HCDG series are ranked according to their density. Among them,

https://doi.org/10.1021/prechem.5c00020
Precis. Chem. XXXX, XXX, XXX−XXX

Table 1. Space Group, Density (ρ), and Primitive Cell of 21 SDCCs[a]

Label	Symmetry group	Density (g/cm^3)	Structures	Label	Symmetry group	Density (g/cm^3)	Structures	Label	Symmetry group	Density (g/cm^3)	Structures
CNTC-2	C2/c	2.248	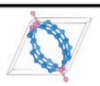	LDCG-6	P2/m	2.910		3D(4,0)-III	Cccm	3.274	
Graphite-3	$P6_3/mmc$	2.258		LDCG-7	Cmcm	2.948		HDCG-5	P2/m	3.287	
LDCG-1	Pm	2.662		LDCG-8	Pbam	2.985		HDCG-6	Cmcm	3.303	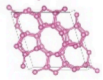
LDCG-2	Fmmm	2.736	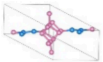	LDCG-9	P2/m	3.000		HDCG-7	Cccm	3.362	
LDCG-3	C2/m	2.736		HDCG-1	Cmcm	3.042		HDCG-8	P2/c	3.403	
Hex-C_{24}	$P6_3/mcm$	2.767		HDCG-3	Cmcm	3.158	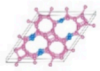	DWHR	C2/m	3.431	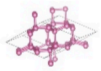
L5-2	$P2_1/m$	2.888	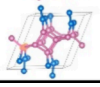	HDCG-4	$P2_1/m$	3.254		Lonsdaleite	$P6_3/mmc$	3.531	

[a]3-fold coordination carbon atoms are marked as blue and 4-fold coordination carbon atoms are marked as pink.

Structures h, s and y cover the previously reported Hex-C_{24},[39] 3D(4,0)-III,[13] and Lonsdaleite,[40] respectively. In these structures, carbon bonding experiences a gradual transition from sp^2 hybridization to sp^3 hybridization. Notably, there are multiple configurations in which sp^2 and sp^3 hybridizations exist simultaneously, highlighting the complexity and diversity of the bonding environments within these structures.

The energy of 25 types of structures obtained is presented in Figure 2a, calculated relative to the energy of AB stacking graphite. The energy values of the same type of structure have been averaged. We can see that as the density increases, the energy tends to rise first and then decrease. HDCG-1 type has the highest relative energy among all structures, with an average value of 0.499 eV. For comparison, the average relative energy of the initial SWNTs structure is 0.512 eV, and the relative energy of C_{60} fullerene is 0.405 eV. That is, all 25 types of structures have a lower energy than the initial SWNTs, showing better thermodynamic stability. These 25 types of structures are compared with the database SACADA,[41] also shown in Figure 2a. Four types of structures have been reported in SACADA (marked in red), while others are not (marked in blue). The graphite-type structure is marked half red and half blue since some of this type of structure has been reported.[42,43] One of the CNTC series coincides with a previous report,[44] but has not been found in the SACADA database.

The averaged density of SDCCs is found to be sensitive to the initial SWNT type and the pressure, as shown in Figure 2b. For the same type of initial SWNT structure, a higher pressure causes a higher density of the final structure in the SSW search. At the same time, as the chirality index n of SWNTs increases (corresponding to larger diameter), the pressure required to form the structure with the same density, e.g., 3.0 g cm^{-3}, increases first (n = 4−9) and remains almost constant (n = 10−12). In addition, the density of the final structures derived from small diameter SWNTs (n = 4−9) changes rapidly with the change of pressure, and when the diameter is large enough (n = 10−12), the density of the final structures is almost constant in the range of 20−40 GPa. Thus, SWNTs with a small diameter are more sensitive to pressure loading than large-diameter SWNTs. Our results have shown that the density of the final structures can be effectively controlled by changing the pressure loading and the initial SWNT diameter, providing guidance for the experimental synthesis of SDCCs with different densities.

Twenty-one structures were selected to evaluate their stability, electronic and mechanical properties. Primitive cells of selected structures and relevant information are shown in Table 1. To examine the thermal stability, we performed AIMD simulations at 300 or 1000 K for 5 ps, as shown in Figures S26−S29. All 21 structures remain almost intact after heating at 300 K and can withstand high temperatures of up to 1000 K, verifying the thermal stability of the SDCCs. To examine the dynamic stability, phonon spectra were calculated, as shown in Figures S30−S31. There are no obvious imaginary modes throughout the whole Brillouin zone for all 21 structures, suggesting that these structures are dynamically stable.

To explore the electronic properties of SDCCs, the band structure and density of states at the PBE level were evaluated. The calculations show that 9 of the 21 structures are metallic, and the others are semiconductors. The band gap of the semiconducting SDCCs ranges from 0.2 to 3.3 eV, including direct and indirect band gaps, as shown in Figure 3a. Very interestingly, the band gap value is found to be related to the density of the structure. When the density is less than 3 g cm^{-3}, the structures are mostly metallic or have a band gap around 0 eV. A sudden leap of the band gap value is observed at ∼3 g cm^{-3}, above which the band gap is maintained at around 3 eV under the PBE level. Since the PBE functional usually underestimates the band gap of a semiconductor, the hybrid functional HSE06 was used for a better evaluation, leading to a larger band gap with an increase of about 1 eV, as shown in Figure 3b-j. Four structures (LDCG-3, LDCG-8, HDCG-3,

https://doi.org/10.1021/prechem.5c00020
Precis. Chem. XXXX, XXX, XXX−XXX

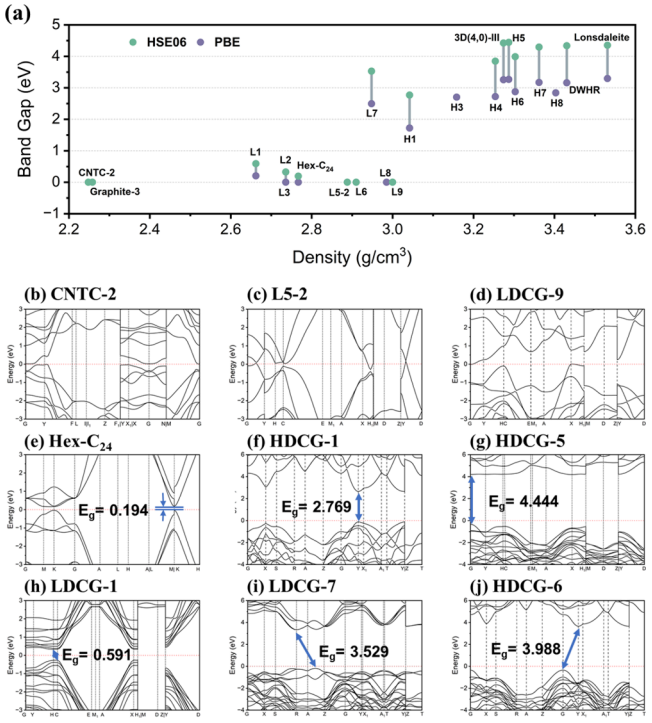

Figure 3. (a) Energy band gaps of SDCCs; (b-j) Band structure of SDCCs based on HSE06 simulations.

HDGC-8) were discarded because they are too large for HSE calculation. Among the calculated 17 structures, 5 are metallic and 12 are semiconductive, with band gaps ranging from 0.2 to 4.4 eV. In addition, we found that the previously reported metallic carbon structure Hex-C_{24},[39] which is identified under the PBE level, exhibits semiconducting properties with a band gap value of 0.194 eV under the HSE06 level. The diversity of the electronic properties of these structures opens possibilities for applications in carbon-based electronic devices. More information about electronic band structure and density of states can be found in Figure S32−S37.

Besides the electronic properties, the mechanical properties of the SDCCs are another important parameter for the carbons derived from CNTs. Especially, superhard materials possess broad application prospects in aerospace, military, metallurgy, and other high-pressure extreme environments.[45] As shown in Figure 4, the calculated modulus and hardness of SDCCs are mostly in the range between graphite and diamond, where the modulus and hardness are linearly correlated to the density. The coefficients of determination in linear fit (R^2) for shear modulus (G), bulk modulus (B), Young's modulus (Y) and Vickers hardness (Hv) are higher than 0.9. The R^2 of Y reaches 0.95. Our observation shows a high consistence to the finding of Blatov et al., in which a correlation between density and bulk/shear moduli in carbon materials was reported.[46] The Pearson correlation coefficient (PCC) between density characteristics and modulus of elasticity in our work is as high as 0.92.[47] The above results have shown that density may be an efficient descriptor for both the mechanical and electronic properties. Moreover, 13 superhard structures, i.e., LDCG-7, LDCG-8, LDCG-9, HDCG-1, HDCG-3, HDCG-4, 3D(4,0)-III, HDCG-5, HDCG-6, HDCG-7, HDCG-8, DWHR, Lonsdaleite, with H_v > 40 GPa[48] and one ductile structure, LDCG-3, with Pugh's Ratio[49] G/B < 0.57 are found. The Vickers hardness values of LDCG-2, L5−2, and LDCG-6 are comparable to those of Tri-C_{54}, Orth-C_{72}, and h-Carbon[50] (approximately 30 GPa); the hardness of HDCG-3 is similar to those of T-carbon[51] and 3D-(4,0)[17] (around 60 GPa). In addition, the hardness of HDCG-8 and DWHR aligns closely with that of M-carbon,[52] 3D-(4,4)[17] or 3D (6,0)-I[13] (approximately 80 GPa).

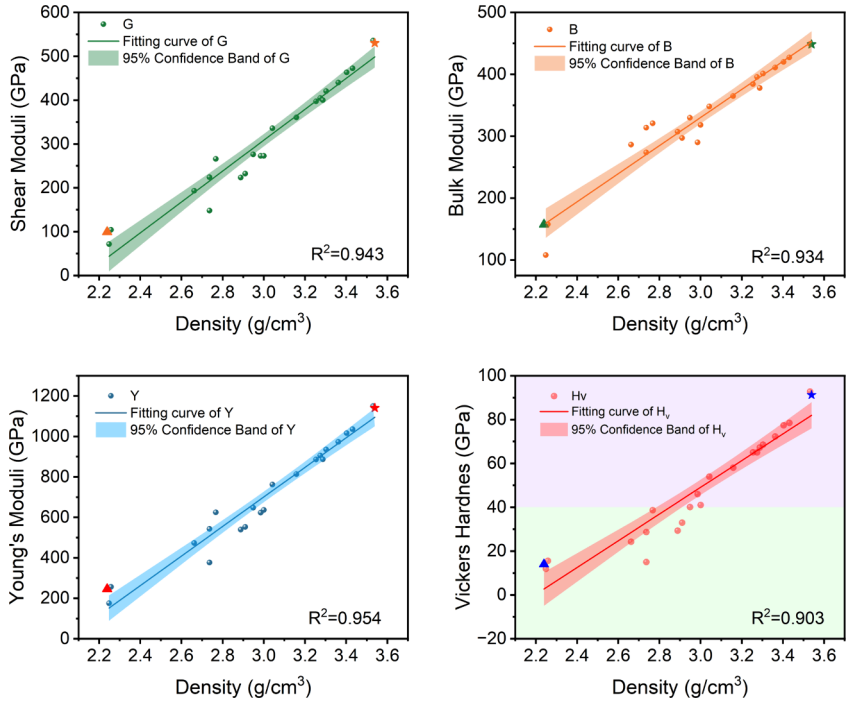

Figure 4. Calculated (a) shear modulus G (GPa), (b) bulk modulus B (GPa), (c)Young's modulus Y (GPa) and (d) Vickers hardness Hv (GPa) of SDCCs.

https://doi.org/10.1021/prechem.5c00020
Precis. Chem. XXXX, XXX, XXX−XXX

In order to efficiently identify these novel carbon structures in future experiments, we further simulated their XRD patterns, as shown in Figure S38. For the layered structure (Graphite-3, GCCS, CNTC-2, and GWHR), the main peak is situated at approximately 26°, akin to the (002) characteristic peak in graphite, reflecting the stacking between graphitic layers;[53] For other SDCCs, there is a distinct peak appearing at around 43°, similar to the (002) diffraction peak in Lonsdaleite.[54]

4. CONCLUSION

In conclusion, we obtained plenty of stable or metastable structures by compressing zigzag SWNT arrays, which include thousands of atoms, using the SSW-NN method. The obtained SDCCs were classified into 25 types of structures, most of which have been reported for the first time. Small-diameter SWNTs were found to be more sensitive to pressure loading than large-diameter SWNTs. A subset of obtained structures was selected to calculate their thermodynamic and dynamical stability and electronic and mechanical properties under DFT level. AIMD simulations and phonon spectrum calculations confirmed their stability under ambient conditions. The SDCCs consist of 9 metallic and 12 semiconductive structures with direct or indirect band gaps ranging from 0.2 to 4.4 eV. Including 13 superhard structures and 1 ductile structure, the structures show a linear correlation between mechanical properties and density, illustrating that density can be a potential descriptor. Our study provides a comprehensive understanding of the structural evolution of SWNTs under pressure, expanding the family of SDCCs, and exploring plenty of interesting SWNTs-derived novel structures with abundant physical properties.

■ ASSOCIATED CONTENT

Supporting Information

The Supporting Information is available free of charge at https://pubs.acs.org/doi/10.1021/prechem.5c00020.

Energy evolution path and intermediate structures, AIMD simulation results, phonon dispersion relations, electronic band structures and density of states, mechanical properties, crystallographic information, and XRD of SDCC (PDF)

The structures reported in article (https://github.com/xsq5616/CNTstructure2025)

■ AUTHOR INFORMATION

Corresponding Authors

Kun Ni − *Department of Materials Science and Engineering, School of Chemistry and Materials Science, & Hefei National Research Center for Physical Sciences at the Microscale, & State Key Laboratory of Precision and Intelligent Chemistry, University of Science and Technology of China, Hefei, Anhui 230026, China*; Email: nikun@ustc.edu.cn

Yanwu Zhu − *Department of Materials Science and Engineering, School of Chemistry and Materials Science, & Hefei National Research Center for Physical Sciences at the Microscale, & State Key Laboratory of Precision and Intelligent Chemistry, University of Science and Technology of China, Hefei, Anhui 230026, China*; orcid.org/0000-0002-7505-1502; Email: zhuyanwu@ustc.edu.cn

Author

Shuqi Xie − *Department of Materials Science and Engineering, School of Chemistry and Materials Science, & Hefei National Research Center for Physical Sciences at the Microscale, & State Key Laboratory of Precision and Intelligent Chemistry, University of Science and Technology of China, Hefei, Anhui 230026, China*

Complete contact information is available at: https://pubs.acs.org/10.1021/prechem.5c00020

Notes

The authors declare no competing financial interest.

■ ACKNOWLEDGMENTS

This work was supported by the National Natural Science Foundation of China (Nos. 52273234, 52325202); The Fundamental Research Funds for the Central Universities (WK2060000098, WK9990000170) and the open research fund of State Key Laboratory of Precision and Intelligent Chemistry (KY2490000300). The Supercomputing Center of USTC and the Hefei Advanced Computing Center is appreciated. Shengcai Zhu is appreciated for his technical support.

■ REFERENCES

(1) Novoselov, K. S.; Geim, A. K.; Morozov, S. V.; Jiang, D.; Zhang, Y.; Dubonos, S. V.; Grigorieva, I. V.; Firsov, A. A. Electric Field Effect in Atomically Thin Carbon Films. *Science* **2004**, *306* (5696), 666−669.

(2) Kroto, H. W.; Allaf, A. W.; Balm, S. P. C60: Buckminsterfullerene. *Chem. Rev.* **1991**, *91* (6), 1213−1235.

(3) Iijima, S. Helical microtubules of graphitic carbon. *Nature* **1991**, *354* (6348), 56−58.

(4) Rathinavel, S.; Priyadharshini, K.; Panda, D. A review on carbon nanotube: An overview of synthesis, properties, functionalization, characterization, and the application. *Materials Science and Engineering: B* **2021**, *268*, No. 115095.

(5) Merlen, A.; Toulemonde, P.; Le Floch, S.; Montagnac, G.; Hammouda, T.; Marty, O.; San Miguel, A. High pressure−high temperature synthesis of diamond from single-wall pristine and iodine doped carbon nanotube bundles. *Carbon* **2009**, *47* (7), 1643−1651.

(6) Khabashesku, V. N.; Gu, Z.; Brinson, B.; Zimmerman, J. L.; Margrave, J. L.; Davydov, V. A.; Kashevarova, L. S.; Rakhmanina, A. V. Polymerization of Single-Wall Carbon Nanotubes under High Pressures and High Temperatures. *J. Phys. Chem. B* **2002**, *106* (43), 11155−11162.

(7) Popov, M.; Kyotani, M.; Nemanich, R. J.; Koga, Y. Superhard phase composed of single-wall carbon nanotubes. *Phys. Rev. B* **2002**, *65* (3), 033408.

(8) Wang, Z.; Zhao, Y.; Tait, K.; Liao, X.; Schiferl, D.; Zha, C.; Downs, R. T.; Qian, J.; Zhu, Y.; Shen, T. A quenchable superhard carbon phase synthesized by cold compression of carbon nanotubes. *Proc. Natl. Acad. Sci. U. S. A.* **2004**, *101* (38), 13699−13702.

(9) Kohn, W.; Sham, L. J. Self-Consistent Equations Including Exchange and Correlation Effects. *Phys. Rev.* **1965**, *140* (4A), A1133−A1138.

(10) Hohenberg, P.; Kohn, W. Inhomogeneous Electron Gas. *Phys. Rev.* **1964**, *136* (3B), B864−B871.

(11) Clark, S. J.; Segall, M. D.; Pickard, C. J.; Hasnip, P. J.; Probert, M. I. J.; Refson, K.; Payne, M. C. First principles methods using CASTEP. *Zeitschrift für Kristallographie - Crystalline Materials* **2005**, *220* (5−6), 567−570.

(12) Umemoto, K.; Wentzcovitch, R. M.; Saito, S.; Miyake, T. Body-centered tetragonal C4: a viable sp3 carbon allotrope. *Phys. Rev. Lett.* **2010**, *104* (12), No. 125504.

(13) Hu, M.; Zhao, Z.; Tian, F.; Oganov, A. R.; Wang, Q.; Xiong, M.; Fan, C.; Wen, B.; He, J.; Yu, D. Compressed carbon nanotubes: A family of new multifunctional carbon allotropes. *Sci. Rep.* **2013**, *3* (1), 1331.
(14) Wang, Y.; Lv, J.; Zhu, L.; Ma, Y. Crystal structure prediction via particle-swarm optimization. *Phys. Rev. B* **2010**, *82* (9), 094116.
(15) Wang, Y.; Lv, J.; Zhu, L.; Ma, Y. CALYPSO: A method for crystal structure prediction. *Comput. Phys. Commun.* **2012**, *183* (10), 2063−2070.
(16) Zhao, Z.; Xu, B.; Zhou, X.-F.; Wang, L.-M.; Wen, B.; He, J.; Liu, Z.; Wang, H.-T.; Tian, Y. Novel Superhard Carbon: C-Centered OrthorhombicC8. *Phys. Rev. Lett.* **2011**, *107* (21), 215502.
(17) Zhao, Z.; Xu, B.; Wang, L.-M.; Zhou, X.-F.; He, J.; Liu, Z.; Wang, H.-T.; Tian, Y. Three Dimensional Carbon-Nanotube Polymers. *ACS Nano* **2011**, *5* (9), 7226−7234.
(18) Hu, K.; Liu, R.; Yao, Z.; Liu, Y.-Y.; Wang, Y.-Y.; Lu, S.-C.; Liu, B.-B. Novel ultrahard carbon structures by cold-compressing tubes. *CrystEngComm* **2021**, *23* (10), 2091−2098.
(19) Shang, C.; Liu, Z. P. Stochastic Surface Walking Method for Structure Prediction and Pathway Searching. *J. Chem. Theory Comput* **2013**, *9* (3), 1838−1845.
(20) Huang, S.-D.; Shang, C.; Zhang, X.-J.; Liu, Z.-P. Material discovery by combining stochastic surface walking global optimization with a neural network. *Chemical Science* **2017**, *8* (9), 6327−6337.
(21) Yu, T.; Zhu, S.-C.; Hou, Y. A novel sp3 carbon allotrope with 4 + 5+6 + 7+8 odd−even ring. *Phys. Chem. Chem. Phys.* **2024**, *26* (33), 22182−22188.
(22) Zhu, S. -c.; Hu, Q. -y. Unraveling the structural transition mechanism of room-temperature compressed graphite carbon. *Phys. Chem. Chem. Phys.* **2021**, *23* (36), 20560−20566.
(23) Zhang, X.-J.; Shang, C.; Liu, Z.-P. From Atoms to Fullerene: Stochastic Surface Walking Solution for Automated Structure Prediction of Complex Material. *J. Chem. Theory Comput.* **2013**, *9* (7), 3252−3260.
(24) Xie, Y.-P.; Zhang, X.-J.; Liu, Z.-P. Graphite to Diamond: Origin for Kinetics Selectivity. *J. Am. Chem. Soc.* **2017**, *139* (7), 2545−2548.
(25) Ni, K.; Pan, F.; Zhu, Y. Structural Evolution of C60 Molecular Crystal Predicted by Neural Network Potential. *Adv. Funct. Mater.* **2022**, *32* (42), 2203894.
(26) Huang, S.-D.; Shang, C.; Kang, P.-L.; Liu, Z.-P. Atomic structure of boron resolved using machine learning and global sampling. *Chemical Science* **2018**, *9* (46), 8644−8655.
(27) Xie, X.-T.; Yang, Z.-X.; Chen, D.; Shi, Y.-F.; Kang, P.-L.; Ma, S.; Li, Y.-F.; Shang, C.; Liu, Z.-P. LASP to the Future of Atomic Simulation: Intelligence and Automation. *Precision Chemistry* **2024**, *2* (12), 612−627.
(28) Hafner, J. Ab-initio simulations of materials using VASP: Density-functional theory and beyond. *J. Comput. Chem.* **2008**, *29* (13), 2044−2078.
(29) Ernzerhof, M.; Scuseria, G. E. Assessment of the Perdew−Burke−Ernzerhof exchange-correlation functional. *J. Chem. Phys.* **1999**, *110* (11), 5029−5036.
(30) Perdew, J. P.; Burke, K.; Ernzerhof, M. Generalized Gradient Approximation Made Simple. *Phys. Rev. Lett.* **1996**, *77* (18), 3865−3868.
(31) Grimme, S.; Antony, J.; Ehrlich, S.; Krieg, H. A consistent and accurate ab initio parametrization of density functional dispersion correction (DFT-D) for the 94 elements H-Pu. *J. Chem. Phys.* **2010**, *132* (15), 154104.
(32) Togo, A.; Oba, F.; Tanaka, I. First-principles calculations of the ferroelastic transition between rutile-type andCaCl2-typeSiO2at high pressures. *Phys. Rev. B* **2008**, *78* (13), 134106.
(33) Krukau, A. V.; Vydrov, O. A.; Izmaylov, A. F.; Scuseria, G. E. Influence of the exchange screening parameter on the performance of screened hybrid functionals. *J. Chem. Phys.* **2006**, *125* (22), 224106.
(34) Hill, R. The Elastic Behaviour of a Crystalline Aggregate. *Proceedings of the Physical Society. Section A* **1952**, *65* (5), 349.
(35) Chen, X.-Q.; Niu, H.; Li, D.; Li, Y. Modeling hardness of polycrystalline materials and bulk metallic glasses. *Intermetallics* **2011**, *19* (9), 1275−1281.
(36) Setyawan, W.; Curtarolo, S. High-throughput electronic band structure calculations: Challenges and tools. *Comput. Mater. Sci.* **2010**, *49* (2), 299−312.
(37) Hinuma, Y.; Pizzi, G.; Kumagai, Y.; Oba, F.; Tanaka, I. Band structure diagram paths based on crystallography. *Comput. Mater. Sci.* **2017**, *128*, 140−184.
(38) Momma, K.; Izumi, F. VESTA 3 for three-dimensional visualization of crystal, volumetric and morphology data. *J. Appl. Crystallogr.* **2011**, *44* (6), 1272−1276.
(39) Bu, H.; Zhao, M.; Dong, W.; Lu, S.; Wang, X. A metallic carbon allotrope with superhardness: a first-principles prediction. *J. Mater. Chem. C* **2014**, *2* (15), 2751−2757.
(40) Frondel, C.; Marvin, U. B. Lonsdaleite, a Hexagonal Polymorph of Diamond. *Nature* **1967**, *214*, 587−589.
(41) Hoffmann, R.; Kabanov, A. A.; Golov, A. A.; Proserpio, D. M. Homo Citans and Carbon Allotropes: For an Ethics of Citation. *Angew. Chem., Int. Ed.* **2016**, *55* (37), 10962−10976.
(42) Bernal, J. D. The structure of graphite. *Proceedings of the Royal Society of London. Series A, Containing Papers of a Mathematical and Physical Character* **1924**, *106* (740), 749−773.
(43) Latil, S.; Henrard, L. Charge carriers in few-layer graphene films. *Phys. Rev. Lett.* **2006**, *97* (3), No. 036803.
(44) Cheng, H.; Pez, G. P.; Cooper, A. C. Spontaneous Cross Linking of Small-Diameter Single-Walled Carbon Nanotubes. *Nano Lett.* **2003**, *3* (5), 585−587.
(45) Riedel, R. *Handbook of ceramic hard materials*; Wiley-VCH, 2000.
(46) Blatov, V. A.; Yang, C.; Tang, D.; Zeng, Q.; Golov, A. A.; Kabanov, A. A. High-throughput systematic topological generation of low-energy carbon allotropes. *npj Computational Materials* **2021**, *7* (1), 15.
(47) Tong, W.; Wei, Q.; Yan, H.-Y.; Zhang, M.-G.; Zhu, X.-M. Accelerating inverse crystal structure prediction by machine learning: A case study of carbon allotropes. *Frontiers of*. *Physics* **2020**, *15* (6), 63501.
(48) Haines, J.; Léger, J.; Bocquillon, G. Synthesis and Design of Superhard Materials. *Annu. Rev. Mater. Res.* **2001**, *31*, 1−23.
(49) Pugh, S. F. Relations between the elastic moduli and the plastic properties of polycrystalline pure metals. *London, Edinburgh, and Dublin Philosophical Magazine and Journal of Science* **1954**, *45* (367), 823−843.
(50) Hu, M.; Pan, Y.; Luo, K.; He, J.; Yu, D.; Xu, B. Three dimensional graphdiyne polymers with tunable band gaps. *Carbon* **2015**, *91*, 518−526.
(51) Sheng, X.-L.; Yan, Q.-B.; Ye, F.; Zheng, Q.-R.; Su, G. T-Carbon: A Novel Carbon Allotrope. *Phys. Rev. Lett.* **2011**, *106* (15), 155703.
(52) Li, Q.; Ma, Y.; Oganov, A. R.; Wang, H.; Wang, H.; Xu, Y.; Cui, T.; Mao, H.-K.; Zou, G. Superhard Monoclinic Polymorph of Carbon. *Phys. Rev. Lett.* **2009**, *102* (17), 175506.
(53) Popova, A. N. Crystallographic analysis of graphite by X-Ray diffraction. *Coke and Chemistry* **2017**, *60* (9), 361−365.
(54) Hanneman, R. E.; Strong, H. M.; Bundy, F. P. Hexagonal Diamonds in Meteorites: Implications. *Science* **1967**, *155* (3765), 995−997.

https://doi.org/10.1021/prechem.5c00020
Precis. Chem. XXXX, XXX, XXX−XXX